Title: Development of an RT-RPA assay for La Crosse virus detection provides insights into age-dependent neuroinvasion in mice

Authors: Lily Lumkong[1], Reem Alatrash[1], Sainetra Sridhar[1], Prince Baffour Tonto[1], Bobby Brooke Herrera[1,2]

Affiliations:

[1]Rutgers Global Health Institute, Rutgers University, New Brunswick, NJ, USA

[2]Department of Medicine, Division of Allergy, Immunology, and Infectious Diseases, and Child Health Institute of New Jersey, Rutgers Robert Wood Johnson Medical School, Rutgers University, New Brunswick, NJ, USA

***Corresponding Author**: BBH, bherrera@globalhealth.rutgers.edu

Keywords: La Crosse virus, Reverse transcription recombinase polymerase amplification, Lateral flow assay, Neuroinvasion, Age-susceptible mouse model

Abstract

Background: La Crosse virus (LACV) is a mosquito-borne arbovirus responsible for pediatric encephalitis in North America, predominantly affecting children under 16 years. Early and accurate diagnosis is critical to reducing morbidity in this vulnerable population. However, existing molecular and serological methods are limited in sensitivity, specificity, and accessibility.

Methods: To address these limitations, we developed a reverse transcription recombinase polymerase amplification (RT-RPA) assay for LACV detection. Primers targeting the divergent M segment of the LACV genome were designed and screened for optimal performance. The assay's analytical sensitivity was evaluated through serial dilutions of LACV RNA prior to reverse transcription, while specificity was assessed using reverse transcribed RNA from related or geographically relevant arboviruses. We further adapted the RT-RPA test into a lateral flow assay (LFA) format for potential point-of-care use. Additionally, we employed a murine model to explore the age-dependent dynamics of LACV neuroinvasion and clearance, with the virus detected using RT-RPA and reverse transcription quantitative polymerase change reaction (RT-qPCR).

Results: Primer screening identified an optimal primer pair that amplified LACV cDNA within 20 minutes at 39°C, with a limit of detection (LOD) of 100 copies. The assay demonstrated high specificity, with no amplification of related or other geographically relevant arboviruses. Integration of the RT-RPA test into an LFA format preserved the LOD and specificity, enabling visual detection via test strips. In the murine model, weanling

mice exhibited LACV neuroinvasion as early as 4 days post-infection (dpi), with sustained detection between 5-7 dpi. In adult mice, neuroinvasion was first detected at 5 dpi, plateauing between 6-10 dpi, and cleared entirely by 20 dpi in surviving animals.

Conclusions: This study establishes the RT-RPA assay as an efficient, specific, and sensitive diagnostic platform for LACV, with potential for adaptation into field-deployable LFA tests. Moreover, our findings provide valuable insights into the age-dependent dynamics of LACV neuroinvasion and clearance, informing future diagnostic and therapeutic strategies.

60 **Background**

61 La Crosse virus (LACV) is a single-stranded, negative-sense virus within the
62 *Peribunyaviridae* family, order *Bunyavirales*, and is classified under the California
63 serogroup (CSG) viruses (1, 2). Members of this viral family possess a distinctive tri-
64 segmented genome composing the small (S), medium (M), and large (L) segments. The S
65 segment of LACV encodes both the nucleocapsid (N) protein and a nonstructural protein
66 (NSs) implicated in the disruption of host innate immune responses (3, 4). The M segment
67 encodes glycoproteins Gn and Gc, which mediate viral attachment and entry, alongside a
68 nonstructural protein (NSm) crucial for virion assembly (5). The L segment encodes the
69 RNA-dependent RNA polymerase (RdRp), an enzyme integral to viral genome transcription
70 and replication (6-8).

71 LACV was first identified in La Crosse, Wisconsin in the 1960s, and has since
72 remained endemic in North America, particularly in the Midwestern and Eastern United
73 States, including the Appalachian corridor (9). Its principal vector is the Eastern treehole
74 mosquito, *Aedes triseriatus*, although more recent data indicate that *Aedes albopictus* and
75 *Aedes japonicus* may also contribute to transmission, raising concerns about geographic
76 expansion (10-12). Between 2003 and 2023, the Centers for Disease Control and
77 Prevention (CDC) documented 1,266 LACV-related hospitalizations in the United States –
78 most of which affected pediatric patients – yet the actual incidence is likely
79 underestimated due to underreporting and diagnostic limitations (7, 13, 14). Furthermore,
80 snowshoe hare virus (SSHV) – a closely related CSG virus that shares approximately 89%
81 sequence identity with LACV – circulates endemically in Canada and has also been

82 associated with outbreaks in young populations, highlighting that arboviruses within the
83 CSG pose a broad threat to populations across North America (15, 16).

84 Human infections with LACV exhibit a wide spectrum of outcomes. While most
85 cases remain asymptomatic or present as mild febrile illness, a subset of infections
86 progress to severe central nervous system (CNS) involvement, resulting in encephalitis,
87 seizures, altered mental status, and, in rare instances, coma or fatality (17). Children under
88 16 years of age are particularly susceptible to adverse outcomes, a pattern attributed in
89 part to differences in immune responses and blood brain barrier function (10, 18-23).

90 Despite its clinical importance, LACV remains difficult to diagnose. Conventional
91 methods such as reverse transcription quantitative polymerase chain reaction (RT-qPCR)
92 provide high sensitivity and specificity during peak viremia, yet its utility diminishes once
93 viral titers wane (13, 24-27). Serological tools, including enzyme-linked immunosorbent
94 assays (ELISAs), can identify LACV-specific antibodies, but often require confirmatory
95 plaque reduction neutralization tests (PRNTs) to differentiate infections from LACV and
96 closely related viruses (28). Moreover, the absence of commercially available LACV-
97 specific RT-qPCRs and ELISAs, and the labor-intensive nature of PRNTs, limit the scalability
98 of these approaches, especially in areas with restricted diagnostic resources.

99 To address these diagnostic hurdles, recombinase polymerase amplification (RPA)
100 has emerged as a promising isothermal nucleic acid amplification technology (29). By
101 functioning at 37-42°C and completing amplification in as few as 20 minutes, RPA reduces
102 the need for specialized equipment. This method employs recombinase enzymes to bind

103 primers to homologous sequences, single-stranded DNA-binding proteins to stabilize the
104 resulting complexes, and strand-displacing polymerases to drive rapid amplification (30-
105 32). When combined with reverse transcription (RT-RPA), the method allows rapid
106 detection of RNA viruses like LACV through an initial conversion of RNA into cDNA.
107 Furthermore, RPA amplicons can be evaluated using standard gel electrophoresis or via
108 lateral flow assays (LFAs), the latter providing near-instantaneous visual results suitable for
109 field-based or point-of-care settings (27, 33). LFAs capitalize on capillary action within a
110 nitrocellulose strip, where labeled detection reagents bind to specific target amplicons,
111 generating visible test and control lines (34-36).

112 In addition to the critical need for improved diagnostics, LACV exhibits age-
113 dependent pathogenicity that requires further investigation. Notably, the age-dependent
114 disease severity observed in humans is recapitulated in murine models, where weanling (3
115 week old) mice display higher mortality rates and more pronounced CNS pathology
116 between 5-7 days post-infection (dpi) compared to adult (≥8 week old) mice with minimal
117 to no death (7, 9, 21, 37, 38). While the pathogenesis of LACV has been relatively well
118 studied in mice and other mammals, limited data are available regarding the temporal
119 dynamics of LACV neuroinvasion into the CNS and/or brain (15, 39, 40).

120 In this study, we describe the development and validation of an RT-RPA assay to
121 detect LACV with high sensitivity and specificity. We also utilize an age-susceptible mouse
122 model to characterize the temporal progression of LACV infection in the brain, exploring
123 how host age influences both neuroinvasion and viral clearance. Our study seeks to

124 enhance early detection in endemic regions and improve the broader understanding of
125 host-pathogen interactions in LACV encephalitis.

126 **Methods**

127 **Multiple sequence alignments and primer/probe design**

128 Percent identity matrix analysis was performed on the S, M, and L segments from a
129 panel of CSG viruses. These included LACV (GenBank accession number: EF485031.1),
130 SSHV (GenBank accession number: EU262553.1), Khatanga virus (GenBank accession
131 number: KT288294.1), California Encephalitis virus (GenBank accession number:
132 KX817313.1), San Angelo virus (GenBank accession number: KX817331.1), Lumbo virus
133 (GenBank accession number: KX817325.1), Tahnya virus (GenBank accession number:
134 EU622819.2), and Jamestown Canyon virus (GenBank accession number: HM007351.1).
135 Multiple sequence alignments and homology analyses were generated using Clustal
136 Omega (version 1.2.4). The resulting sequence alignments were subjected to phylogenetic
137 analysis by constructing maximum-likelihood trees based on the Tamura-Nei model and
138 500 bootstrapping replications using Mega11 software.

139 Primers were manually designed using SnapGene software (version 8.0.1)
140 (Supplementary Table 1), adhering to established RPA guidelines that limit the primer
141 length to 30-35 bases, maintain 40-60% GC content, and minimize palindromic or
142 repetitive sequences (32). Primer candidates were initially tested in silico for hairpin and
143 dimer formation. Those meeting these criteria underwent validation at three temperatures,

144 including 37°C, 39°C, and 42°C, for 20 minutes. The primer pair that yielded the strongest,
145 most specific band was used in subsequent experiments.

146 **RNA Extraction**

147 The PureLink Viral RNA/DNA Mini kit (ThermoFisher) was used for RNA extraction
148 from LACV (BEI Resources: NR-540, GenBank accession number: GCA_004789695.1),
149 SSHV (BEI Resources: NR-535, GenBank accession number: GCA_004789895.1), DENV-1
150 (BEI Resources: Hawaii strain, GenBank accession number: KM204119.1), DENV-2 (BEI
151 Resources: DakArA1247 strain, GenBank accession number: EF105383), DENV-3 (BEI
152 Resources: DENV-3/US/BID-V1043/2006 strain, GenBank accession number: EU482555),
153 DENV-4 (BEI Resources: H241 strain, GenBank accession number: AY947539), ZIKV (BEI
154 Resources: DAK AR 41524 strain, GenBank accession number: KX601166), WNV (BEI
155 Resources: Bird114 strain, GenBank accession number: GU827998.1), and YFV (BEI
156 Resources: YFV17D strain, GenBank accession number: MG051217.1), following the
157 manufacturer's instructions. Additionally, RNA from mouse brains was extracted using the
158 RNeasy Lipid tissue Mini Kit (Qiagen), following the manufacturer's instructions. The
159 concentration of the RNA extracts was determined using a NanoDrop One device
160 (ThermoFisher).

161 **cDNA synthesis and primer screening**

162 Viral RNA was converted to cDNA using the High-Capacity cDNA Reverse
163 Transcription Kit (ThermFisher), following the manufacturer's instructions. 10 µl of
164 extracted RNA was input into a 20 µL cDNA synthesis reaction. For the primer screen, 1 µl

165 of viral cDNA was used as input for primer screens, limit of detection (LOD) test, and cross-
166 reactivity screen RPA reactions. 1 µl of water was used as input for negative controls.

167 **RT-RPA reactions using unlabeled primers**

168 RPA reactions were conducted using the TwistAmp Basic Lyophilized Kit (TwistDx),
169 following the manufacturer's instructions, but were scaled down from a 50 µL reaction to a
170 10 µL reaction. In brief, the lyophilized mix was rehydrated using 29.5 µL of the provided
171 rehydration buffer and 10 µL of nuclease-free water. 7.9 µL of the rehydrated mix was used
172 per 10 µL reaction, along with 0.3 µM of each primer, 280 mM magnesium acetate, and 1µL
173 of cDNA. The reactions were incubated for 20 minutes at either 37°C, 39°C, or 42°C.
174 Diluted reaction products (2:1) were run on a 2.5% agarose gel (BioRad) in 1x TAE buffer
175 (BioRad) for 30 minutes at 100 volts.

176 **RT-RPA reactions using labelled primers**

177 For the hybridization method, reactions were set up as described as above, with one
178 minor change, where the reverse primer was replaced with a reverse primer with a 5'biotin
179 labelled version, with the same primer concentration in the reaction. The hybridization step
180 was performed as described by Qian's hybridization protocol (41), using a probe that was
181 labeled with a 5'-FAM tag (Supplementary Table 1). Following the RPA reaction run, 1 µL of
182 5 µM hybridization probe (final concentration of 0.167 µM) and 19 µL of hybridization buffer
183 (10 mM Tris HCl at pH 8.5) were added to each reaction. This reaction mix was heated to
184 95°C for 3 minutes on the thermocycler and then cooled to room temperature to allow for
185 the hybridization reaction.

186 **Detection of RPA products on LFA strips**

187 The products from the hybridization reactions were processed using the
188 HybriDetect 2T LFA strips (Milenia Biosciences), following the manufacturer's instructions.
189 Unpurified reaction products were diluted in the provided assay buffer (1:15 for
190 hybridization reactions) and applied to the strip. The strip was then immersed in 70 µL of
191 the provided assay buffer and was allowed to react for 10-15 minutes. The strips were
192 imaged using a smartphone camera.

193 **qPCR**

194 cDNA samples derived from mice brains were analyzed by qPCR using PowerTrack
195 SYBR Green kit (ThermoFisher) to detect LACV. The following primers were used: forward
196 (ATTCTACCCGCTGACCATTG) and reverse (GTGAGAGTGCCATAGCGTTG) (15). qPCR was
197 performed using a QuantStudio 3Flex instrument (Applied Biosystems). QuantStudio Real-
198 Time PCR software was used to extract data. GAPDH was used as a control of expression
199 for qPCR samples.

200 **Infection of mice with LACV and timepoint collection**

201 All animal studies were approved by the Rutgers University IACUC (protocol number
202 202300007) and performed in accordance with protocols set forth by the National
203 Institutes of Health *Guide for the Care and Use of Laboratory Animals* and ARRIVE
204 guidelines. Wildtype (C57BL/6) mice were purchased from Jackson Laboratories and
205 maintained in a breeding colony at the Child Health Institute of New Jersey. Weanling (3
206 weeks old) and adult mice (8 weeks old) were inoculated with 10^3 PFU of LACV in

207 phosphate-buffered saline (PBS) intraperitoneally in a volume of 100 µl/mouse. Mice were
208 observed daily for signs of neurological disease. Animals with clinical signs were scored
209 and humanely euthanized if they demonstrated clear signs of neurological disease,
210 including seizures plus lethargy. For the clinical scoring graphs, the percentage of mice
211 with neurological disease was calculated based on the number of weanling or adult mice
212 out of the total number of surviving animals for each age groups. Mice were sacrificed and
213 brains were collected at the following timepoints: 2, 3, 4, 5, and 7 days post-infection (dpi)
214 for weanlings and 4, 5, 6, 7, 10, and 20 dpi for adults and were stored in RNAse away, as
215 previously described (20, 22). Viral RNA was extracted as described.

216 **Rapid test strip image analysis and viral quantification**

217 To estimate viral loads from rapid test strip images, we first established a standard
218 curve using known viral RNA copies. LACV RNA was serially diluted to generate
219 concentrations ranging from 10^6 to 0 copies for RT-RPA testing with results visualization via
220 LFA strips. Resulting test line bands were imaged using under consistent lighting
221 conditions. Image processing and pixel intensity quantification were performed using
222 ImageJ software (NIH) (27, 42-44). The pixel intensity of the test line for each dilution was
223 recorded and plotted against the corresponding viral copy number to generate a standard
224 curve. A linear regression model was fitted to the standard curve, and the equation y =
225 $10^{(m*x+b)}$ was derived, where x represents the pixel intensity, and y corresponds to the
226 estimated viral copy number. This equation was used to interpolate viral loads for test
227 samples based on their measured pixel intensities.

228 The test line intensity for each weanling and adult mouse sample was measured
229 using ImageJ and converted to viral copies using the standard curve equation. Pixel
230 intensities for adult and weanling samples were plotted on the standard curve to estimate
231 viral load dynamics over time. Graphical representations were performed using Python
232 (Matplotlib, NumPy, SciPy, and Seaborn). The standard curve was plotted as a black
233 straight live, generated using linear repression.

234 **Results**

235 **Screening of RT-RPA primer pairs for LACV detection**

236 To identify a genome segment best suited for specific and sensitive detection of
237 LACV, we performed a percentage identity matrix analysis on the S, M, and L segments
238 from a panel of CSG viruses. These included LACV, SSHV, Khatanga virus, California
239 Encephalitis virus, San Angelo virus, Lumbo virus, and Tahnya virus, and one virus from the
240 Melaka virus family, Jamestown Canyon virus. Based on homology analyses of DNA
241 sequences, the S, M, and L segments displayed homology ranging from 76.1-88%, 69-
242 78.8%, and 73.7-81.6%, respectively (Fig. 1, Table 1). Since the M segment exhibited the
243 greatest divergence between LACV and other CSG viruses, we selected it as the target for
244 LACV-specific primer design.

245 Four primer pairs were generated, each producing amplicons of at least 100 base
246 pairs. These primers were tested at 37°C, 39°C, and 42°C for 20 minutes. Primer pair 3 at
247 39°C yielded the clearest and most intense amplification band (208 base pairs [bp]) and
248 was chosen for subsequent optimization (Fig. 2). Primer pair 4 also showed reliable results

249 (240 bp), but was slightly less optimal. Notably, the RT-RPA amplified products were
250 analyzed via agarose gel electrophoresis without prior purification, enabling efficient
251 screening of primer pairs.

252 **Assessing LACV RT-RPA amplification time and analytical sensitivity and specificity**
253 **via gel electrophoresis**

254 After identifying the best performing primer pair, we conducted a time course study
255 to determine the minimal incubation period necessary for effective RT-RPA detection of
256 LACV. Reactions were incubated for 5, 10, 20, and 60 minutes before the amplicons were
257 purified and visualized by agarose gel electrophoresis. Although faint bands appeared as
258 early as 10 minutes, we observed optimal band clarity and intensity at 20 minutes (Fig. 3A).

259 Next, we evaluated the RT-RPA assay's analytical sensitivity using a ten-fold serial
260 dilution of LACV RNA, ranging from 10^5 to 0 input copies in the RT step. The RT-RPA
261 reactions were purified and then assessed via agarose gel electrophoresis. The LOD was
262 established at 100 copies (Fig. 3B), similar to the RT-qPCR assay. To verify the RT-RPA
263 assay's specificity, we tested RNA extracted from other arboviruses, including SSHV,
264 dengue virus serotypes 1-4 (DENV-1-4), Zika virus (ZIKV), West Nile virus (WNV), and yellow
265 fever virus (YFV). Similarly, the RT-RPA reactions were purified and then assessed via
266 agarose gel electrophoresis. No RT-RPA or RT-qPCR amplification occurred in any non-
267 LACV samples, confirming the specificity of our primer pair (Fig. 3C).

268

269

270 **Integration of the LACV RT-RPA assay with an LFA**

271 To enable the potential point-of-care diagnosis of LACV, a lateral flow assay (LFA)
272 was developed and integrated with the LACV RT-RPA assay. We employed the same
273 unlabeled forward primer, but the reverse primer was adapted to contain a 5'-biotin tag,
274 combined with a short hybridization step in which the probe was labeled with a 5'-FAM tag.
275 After RT-RPA and hybridization, the product was exposed to the LFA strip, containing
276 detection lines coated with streptavidin on the test area and anti-rabbit antibody on the
277 control area. Gold nanoparticle-conjugated anti-rabbit-FITC antibodies generated the
278 visual signal upon binding to hybridization product containing the FAM and biotin labels.
279 The LFA exhibited the same LOD of 100 copies (Fig. 4A). Similarly, the LFA also did not
280 cross-react with SSHV and the other geographically relevant arboviruses (Fig. 4B). These
281 results confirm the LFA's utility as a potential rapid and field-deployable tool for LACV
282 detection.

283 **Evaluation of age-dependent detection and clearance of LACV in weanling and adult**
284 **mouse brains**

285 To probe how host age modulates LACV neuroinvasion, we utilized both weanling
286 and adult C57BL/6 mice. Animals were inoculated intraperitoneally with 10^3 plaque forming
287 units (PFU) of LACV, and brains were collected at distinct dpi. Weanling mice were
288 sacrificed and sampled at 2, 3, 4, 5, and 7 dpi, whereas adult mice were sacrificed and
289 sampled at 4, 5, 6, 7, 10, and 20 dpi (Supplementary Fig. 1A). RNA from brains was
290 extracted, reverse transcribed to cDNA, and evaluated using RT-qPCR as well as the newly

291 developed RT-RPA test, with results visualization by LFA strips and agarose gel
292 electrophoresis.

293 We observed that LACV accessed the brains of weanling mice as early as 4 dpi and
294 was detectable in all mice at the 5-7 dpi timepoints (Fig. 5A, Supplementary Fig. 1B). The
295 onset of symptoms coincided with LACV access to the CNS, with abnormal gait observed
296 in 11% (one out of nine remaining weanling mice at 4 dpi), and 100% of the remaining
297 weanlings exhibiting severe neurological symptoms between 5-7 dpi (Fig. 5B). In adult
298 mice, LACV was first detected at 5 dpi, plateauing between 6-10 dpi (Fig. 5C,
299 Supplementary Fig. 1C). By 20 dpi, LACV was undetectable in the surviving adults,
300 suggesting robust viral clearance. In contrast to weanlings, 100% of adults exhibited no
301 symptoms between 4-7 dpi, with abnormal gait observed in 16.7% (one out of six remaining
302 adult mice) at 10 dpi (Fig. 5D). The 20 dpi timepoint included only two mice as one mouse
303 in the 20 dpi cohort succumbed to the infection at 12 dpi and could not be included in the
304 analysis.

305 Furthermore, viral load quantification was derived from a standard curve generated
306 from known LACV RNA copies (Fig. 4A). The standard curve demonstrated a strong
307 correlation between pixel intensity and viral copies ($R^2 > 0.99$), enabling estimation of LACV
308 burden in the brain. Estimated viral copies in weanling brains at peak infection (4-5 dpi)
309 ranged from ~$10^{4.5}$ to ~10^6, consistent with high neuroinvasive potential at early time points
310 (Fig. 6A-B). Peak viral burden in adult brains was notably lower than in weanlings between
311 5-10 dpi, with estimated viral loads between ~10^2 to ~10^3 copies between (Fig. 6A-B).
312 However, there was one adult with high viral load at 10 dpi (Fig. 6A-B).

313 **Discussion**

314 In this study, we developed, optimized, and validated an RT-RPA assay to detect
315 LACV. Traditional RT-qPCR techniques, although highly sensitive, rely on costly equipment
316 and specialized laboratory settings, and often lose sensitivity as viral titers decline (24, 25).
317 Serological tools, meanwhile, necessitate confirmatory plaque reduction neutralization
318 tests (PRNTs) to differentiate among closely related arboviruses—a process that can be
319 time-intensive and cumbersome for large-scale or field-based testing (26, 45). Our RT-RPA
320 assay addresses these limitations by demonstrating efficient and robust LACV detection
321 with a LOD of 100 RNA copies and without cross-reaction. This performance was
322 replicated in both agarose gel electrophoresis and LFA strips, underscoring the assay's
323 versatility and potential utility in resource-constrained environments where on-site
324 diagnostics could significantly improve patient management and epidemiological
325 surveillance.

326 An important aspect of our assay's development was the primer design targeting the
327 M segment. Using bioinformatic analysis of multiple CSG viruses, we observed greater
328 sequence divergence in the M segment between LACV and closely related CSG viruses. By
329 designing primers and a probe that map specifically to these divergent regions, we
330 achieved high specificity without any cross-reactivity against SSHV and other
331 geographically relevant arboviruses (46). These findings confirm that our assay is well
332 suited to environments where multiple arboviruses circulate simultaneously. Moreover, the
333 integrated approach of utilizing an unpurified RT-RPA product for hybridization plus results
334 readout via an LFA strip reliably produced clear test lines, suggesting a potentially

335 straightforward workflow for use in clinics or field settings lacking sophisticated
336 equipment. In future iterations, combining the RT and RPA steps into a single reaction may
337 further streamline testing by potentially eliminating the need for RNA extraction and cDNA
338 synthesis.

339 Beyond its diagnostic innovation, our study provides important new insights into
340 LACV pathogenesis, particularly the impact of host age on the temporal neuroinvasion
341 dynamics. While the progression of LACV neuroinvasion in weanling mice has been well
342 studied, the dynamics in adult mice remained poorly characterized, and a direct
343 comparative analysis between weanlings and adults had not been previously investigated
344 (39). Using a serial euthanasia approach, we assessed LACV detection in the brain of both
345 weanling and adult mice at predefined intervals (2–7 dpi for weanlings; 4–20 dpi for adults).
346 We demonstrated that weanling mice exhibited detectable virus in the brain as early as 4
347 dpi, with sustained high viral loads between 5-7 dpi, and most weanling mice displaying
348 severe CNS pathology by the end of the study window. Conversely, in adult mice, LACV was
349 first detected in the brain at 5 dpi—indicating a delayed onset of neuroinvasion compared
350 to weanlings—and exhibited plateauing levels between 6–10 dpi. Notably, some adults still
351 harbored detectable virus at 10 dpi, yet all surviving adults cleared the virus within the
352 brain completely by 20 dpi.

353 While survival outcomes were not directly assessed in this study due to our serial
354 euthanasia design, extensive prior research has consistently demonstrated that weanlings
355 typically succumb by 7 dpi, whereas adult mice exhibit minimal to no mortality (20-22, 39,
356 40). However, our estimation of LACV burden based on LFA strip image analysis

357 demonstrated notably higher viral loads in the brains of weanlings compared to adults.
358 Together with the current study, these findings suggest that adult mice experience a slower
359 initial spread of virus into the CNS relative to weanlings, potentially allowing more time for
360 immune responses to mitigate viral replication and promote survival. Although further
361 immunological assays would be required to pinpoint the specific immune responses
362 involved, the delayed neuroinvasion and ultimately effective viral clearance in adults likely
363 underlie their more favorable clinical outcomes compared to younger hosts (21). Our
364 recent analysis of T cell immunity demonstrates significant disparities in the cellular
365 response to LACV in weanling and adult mice (47). Adult mice mount significantly more
366 polyfunctional $CD4^+$ and $CD8^+$ T cell responses compared to minimal responses in
367 weanlings (47).

368 Despite the strengths of our study, several limitations should be acknowledged.
369 First, while our RT-RPA assay demonstrated high sensitivity and specificity for LACV
370 detection, we did not evaluate its performance using human clinical samples. Given the
371 rarity of confirmed LACV cases and the challenges in obtaining clinical specimens,
372 validation in patient samples remains an important next step. Additionally, our study relied
373 on in vitro and murine models to assess viral detection and neuroinvasion. While these
374 models provide valuable insights, human pathophysiology may differ, necessitating further
375 validation in human-derived tissues or clinical studies. Another limitation is that while our
376 assay successfully distinguished LACV from closely related CSG viruses, broader
377 validation against a wider panel of co-circulating arboviruses would further strengthen its
378 diagnostic utility.

379 Furthermore, a potential limitation of RT-RPA/LFA is reduced sensitivity at early and
380 late stages of infection, when viral titers are low. While our assay demonstrated a limit of
381 detection of 100 copies, further optimization is needed to enhance sensitivity for clinical
382 applications. Future improvements could include incorporating a pre-amplification step to
383 increase RNA yield, using fluorescent or nanoparticle-based lateral flow detection to
384 enhance signal amplification, and developing a multiplexed RT-RPA approach targeting
385 multiple genomic regions to improve detection across a range of viral loads. Finally, future
386 work should explore the integration of RT and RPA into a single-tube reaction to further
387 simplify the assay workflow, enhancing its feasibility for field deployment.

388 **Conclusion**

389 Taken together, our work underscores a dual contribution to the field: we introduce a
390 highly sensitive and specific RT-RPA assay for LACV detection, and we leverage this assay
391 to enhance our understanding of age-dependent neuroinvasion in a murine model.
392 Importantly, the RT-RPA method is amenable to further refinements, such as one-step RT-
393 RPA protocols or improved probe chemistries, which could streamline its use under
394 outbreak conditions. From a public health perspective, quicker diagnoses in endemic or
395 high-risk regions would facilitate timely interventions, especially for pediatric populations
396 at greatest risk of severe outcomes. Meanwhile, our findings on the timing and efficiency of
397 viral invasion in adult versus weanling brains point toward an inherent advantage conferred
398 by age-related immune maturity, reinforcing the notion that prophylactic or early
399 therapeutic measures could be particularly impactful in children. Overall, these

advancements promise to mitigate the burden of LACV disease and enrich our broader comprehension of arboviral neuroinvasion.

Ethics approval and consent to participate

Not applicable.

Consent for publication

Not applicable.

Availability of data and material

All data generated or analyzed during this study are included in the published article and its supplementary information files.

Competing interests

BBH is a co-founder of Mir Biosciences, Inc., a biotechnology company focused on T cell-based diagnostics and vaccines for infectious diseases, cancer, and autoimmunity.

Funding

Funding was provided by the New Jersey Health Foundation (IFHA18-24). The funders had not role in the conceptualization, design, data collection, analysis, decision to publish, or preparation of the manuscript.

Author Contributions

LL designed probes and primers, planned, ran most of the experiments described above, analyzed experimental data, and wrote the original draft of manuscript. RA assisted

419 with mouse infections, mouse monitoring, and brain collection. SS helped with the
420 development of primers, probes, and protocol optimization. PBT helped with RNA
421 extractions. BBH developed the ideas for the project, as well as supervised the work, and
422 planned and carried out experiments. All authors contributed to the interpretation of the
423 data and played a role in reviewing and editing the manuscript.

424 **Acknowledgements**

425 We would like to thank Rutgers Global Health Institute, Rutgers Robert Wood
426 Johnson Medical School, and The Child Health Institute of New Jersey for their continued
427 support.

428 **References**

429 1. Alatrash R, Herrera BB. The Adaptive Immune Response against Bunyavirales.
430 Viruses. 2024;16(3).
431 2. Evans AB, Peterson KE. Throw out the Map: Neuropathogenesis of the Globally
432 Expanding California Serogroup of Orthobunyaviruses. Viruses. 2019;11(9).
433 3. Soldan SS, Plassmeyer ML, Matukonis MK, Gonzalez-Scarano F. La Crosse virus
434 nonstructural protein NSs counteracts the effects of short interfering RNA. J Virol.
435 2005;79(1):234-44.
436 4. Blakqori G, Delhaye S, Habjan M, Blair CD, Sanchez-Vargas I, Olson KE, et al. La
437 Crosse bunyavirus nonstructural protein NSs serves to suppress the type I interferon
438 system of mammalian hosts. J Virol. 2007;81(10):4991-9.

5. Soldan SS, Hollidge BS, Wagner V, Weber F, Gonzalez-Scarano F. La Crosse virus (LACV) Gc fusion peptide mutants have impaired growth and fusion phenotypes, but remain neurotoxic. Virology. 2010;404(2):139-47.

6. Reese SM, Blitvich BJ, Blair CD, Geske D, Beaty BJ, Black WCt. Potential for La Crosse virus segment reassortment in nature. Virol J. 2008;5:164.

7. Bennett RS, Ton DR, Hanson CT, Murphy BR, Whitehead SS. Genome sequence analysis of La Crosse virus and in vitro and in vivo phenotypes. Virol J. 2007;4:41.

8. Arragain B, Durieux Trouilleton Q, Baudin F, Provaznik J, Azevedo N, Cusack S, et al. Structural snapshots of La Crosse virus polymerase reveal the mechanisms underlying Peribunyaviridae replication and transcription. Nat Commun. 2022;13(1):902.

9. Day CA, Odoi A, Trout Fryxell R. Geographically persistent clusters of La Crosse virus disease in the Appalachian region of the United States from 2003 to 2021. PLoS Negl Trop Dis. 2023;17(1):e0011065.

10. McJunkin JE, Khan RR, Tsai TF. California-La Crosse encephalitis. Infect Dis Clin North Am. 1998;12(1):83-93.

11. Goldman T, Hamer DH. Current Status of La Crosse Virus in North America and Potential for Future Spread. Am J Trop Med Hyg. 2024;110(5):850-5.

12. Haddow AD, Odoi A. The incidence risk, clustering, and clinical presentation of La Crosse virus infections in the eastern United States, 2003-2007. PLoS One. 2009;4(7):e6145.

13. CDC. La Cross virus [Available from: https://www.cdc.gov/la-crosse-encephalitis/about/index.html].

461 14. Gaensbauer JT, Lindsey NP, Messacar K, Staples JE, Fischer M. Neuroinvasive
462 arboviral disease in the United States: 2003 to 2012. Pediatrics. 2014;134(3):e642-50.
463 15. Evans AB, Winkler CW, Peterson KE. Differences in Neuropathogenesis of
464 Encephalitic California Serogroup Viruses. Emerg Infect Dis. 2019;25(4):728-38.
465 16. Lau L, Wudel B, Kadkhoda K, Keynan Y. Snowshoe Hare Virus Causing
466 Meningoencephalitis in a Young Adult From Northern Manitoba, Canada. Open Forum
467 Infect Dis. 2017;4(3):ofx150.
468 17. Boutzoukas AE, Freedman DA, Koterba C, Hunt GW, Mack K, Cass J, et al. La Crosse
469 Virus Neuroinvasive Disease in Children: A Contemporary Analysis of
470 Clinical/Neurobehavioral Outcomes and Predictors of Disease Severity. Clin Infect Dis.
471 2023;76(3):e1114-e22.
472 18. Harding S, Greig J, Mascarenhas M, Young I, Waddell LA. La Crosse virus: a scoping
473 review of the global evidence. Epidemiol Infect. 2018;147:e66.
474 19. Day CA, Byrd BD, Trout Fryxell RT. La Crosse virus neuroinvasive disease: the kids
475 are not alright. J Med Entomol. 2023;60(6):1165-82.
476 20. Basu R, Ganesan S, Winkler CW, Anzick SL, Martens C, Peterson KE, et al.
477 Identification of age-specific gene regulators of La Crosse virus neuroinvasion and
478 pathogenesis. Nat Commun. 2023;14(1):2836.
479 21. Alatrash R, Vaidya V, Herrera BB. Age-specific dynamics of neutralizing antibodies,
480 cytokines, and chemokines in response to La Crosse virus infection in mice. J Virol.
481 2024;98(12):e0176224.

482 22. Basu R, Nair V, Winkler CW, Woods TA, Fraser IDC, Peterson KE. Age influences
483 susceptibility of brain capillary endothelial cells to La Crosse virus infection and cell death.
484 J Neuroinflammation. 2021;18(1):125.
485 23. Teleron AL, Rose BK, Williams DM, Kemper SE, McJunkin JE. La Crosse Encephalitis:
486 An Adult Case Series. Am J Med. 2016;129(8):881-4.
487 24. Wasieloski LP, Jr., Rayms-Keller A, Curtis LA, Blair CD, Beaty BJ. Reverse
488 transcription-PCR detection of LaCrosse virus in mosquitoes and comparison with enzyme
489 immunoassay and virus isolation. J Clin Microbiol. 1994;32(9):2076-80.
490 25. Watzinger F, Ebner K, Lion T. Detection and monitoring of virus infections by real-
491 time PCR. Mol Aspects Med. 2006;27(2-3):254-98.
492 26. Lambert AJ, Nasci RS, Cropp BC, Martin DA, Rose BC, Russell BJ, et al. Nucleic acid
493 amplification assays for detection of La Crosse virus RNA. J Clin Microbiol.
494 2005;43(4):1885-9.
495 27. Salcedo N, Sena BF, Qu X, Herrera BB. Comparative Evaluation of Rapid Isothermal
496 Amplification and Antigen Assays for Screening Testing of SARS-CoV-2. Viruses. 2022;14(3).
497 28. Evans AB, Peterson KE. Cross reactivity of neutralizing antibodies to the encephalitic
498 California Serogroup orthobunyaviruses varies by virus and genetic relatedness. Sci Rep.
499 2021;11(1):16424.
500 29. Daher RK, Stewart G, Boissinot M, Bergeron MG. Recombinase Polymerase
501 Amplification for Diagnostic Applications. Clin Chem. 2016;62(7):947-58.

502 30. Faye M, Abd El Wahed A, Faye O, Kissenkotter J, Hoffmann B, Sall AA, et al. A
503 recombinase polymerase amplification assay for rapid detection of rabies virus. Sci Rep.
504 2021;11(1):3131.
505 31. Vasileva Wand NI, Bonney LC, Watson RJ, Graham V, Hewson R. Point-of-care
506 diagnostic assay for the detection of Zika virus using the recombinase polymerase
507 amplification method. J Gen Virol. 2018;99(8):1012-26.
508 32. Lobato IM, O'Sullivan CK. Recombinase polymerase amplification: Basics,
509 applications and recent advances. Trends Analyt Chem. 2018;98:19-35.
510 33. Sainetra Sridhar PBT, Lily Lumkong, Eduardo Martins Netto, Carlos Brites, Wei-Kung
511 Wang & Bobby Brooke Herrera. RT-RPA as a dual tool for detection and phylogenetic
512 analysis of epidemic arthritogenic alphaviruses. Scientific Reports. 2024;14.
513 34. Jauset-Rubio M, Svobodova M, Mairal T, McNeil C, Keegan N, Saeed A, et al.
514 Ultrasensitive, rapid and inexpensive detection of DNA using paper based lateral flow
515 assay. Sci Rep. 2016;6:37732.
516 35. Shelite TR, Uscanga-Palomeque AC, Castellanos-Gonzalez A, Melby PC, Travi BL.
517 Isothermal recombinase polymerase amplification-lateral flow detection of SARS-CoV-2,
518 the etiological agent of COVID-19. J Virol Methods. 2021;296:114227.
519 36. Ghosh DK, Kokane SB, Gowda S. Development of a reverse transcription
520 recombinase polymerase based isothermal amplification coupled with lateral flow
521 immunochromatographic assay (CTV-RT-RPA-LFICA) for rapid detection of Citrus tristeza
522 virus. Sci Rep. 2020;10(1):20593.

523 37. Davis J, Atkins C, Doyle M, Williams C, Boyce R, Byrd B. Endemic La Crosse Virus
524 Neuroinvasive Disease in North Carolina Residents: 2000-2020. N C Med J. 2024;85(4):289-
525 95.
526 38. Taylor KG, Woods TA, Winkler CW, Carmody AB, Peterson KE. Age-dependent
527 myeloid dendritic cell responses mediate resistance to la crosse virus-induced
528 neurological disease. J Virol. 2014;88(19):11070-9.
529 39. Bennett RS, Cress CM, Ward JM, Firestone CY, Murphy BR, Whitehead SS. La Crosse
530 virus infectivity, pathogenesis, and immunogenicity in mice and monkeys. Virol J.
531 2008;5:25.
532 40. Evans AB, Winkler CW, Peterson KE. Differences in neuroinvasion and protective
533 innate immune pathways between encephalitic California Serogroup orthobunyaviruses.
534 PLoS Pathog. 2022;18(3):e1010384.
535 41. Qian J, Boswell SA, Chidley C, Lu ZX, Pettit ME, Gaudio BL, et al. An enhanced
536 isothermal amplification assay for viral detection. Nat Commun. 2020;11(1):5920.
537 42. Harmon A, Chang C, Salcedo N, Sena B, Herrera BB, Bosch I, et al. Validation of an
538 At-Home Direct Antigen Rapid Test for COVID-19. JAMA Netw Open. 2021;4(8):e2126931.
539 43. Salcedo N, Harmon A, Herrera BB. Pooling of Samples for SARS-CoV-2 Detection
540 Using a Rapid Antigen Test. Front Trop Dis. 2021;2:707865.
541 44. Salcedo N, Reddy A, Gomez AR, Bosch I, Herrera BB. Monoclonal antibody pairs
542 against SARS-CoV-2 for rapid antigen test development. PLoS Negl Trop Dis.
543 2022;16(3):e0010311.

544 45. Calisher CH, Pretzman CI, Muth DJ, Parsons MA, Peterson ED. Serodiagnosis of La
545 Crosse virus infections in humans by detection of immunoglobulin M class antibodies. J
546 Clin Microbiol. 1986;23(4):667-71.
547 46. Pierson TC, Diamond MS. The continued threat of emerging flaviviruses. Nat
548 Microbiol. 2020;5(6):796-812.
549 47. Alatrash R, Herrera BB. Immunodominant structural proteins Gc and N drive T cell-
550 mediated protection against La Crosse virus. bioRxiv. 2025:2025.02. 25.640063.

551

552

553

554

555

556

557

558

559

560

561

562

563 **Tables**

564 **Table 1. Nucleic acid sequence homology of the S, M, and L segments between LACV**

565 **and other related bunyaviruses**

Virus	S Segment Homology	M Segment Homology	L Segment Homology
La Crosse virus	100%	100%	100%
Snowshoe hare virus	88%	78.8%	81.6%
Khatanga virus	87%	77.5%	78%
California encephalitis virus	79.8%	73.6%	76.9%
Tahyna virus	82.2%	73%	77.3%
Lumbo virus	80.7%	72.3%	76.7%
San Angelo virus	80.1%	70.5%	77.1%
Jamestown Canyon virus	76.1%	69%	73.7%

566

567

568

569

570

571

572

573 **Figures**

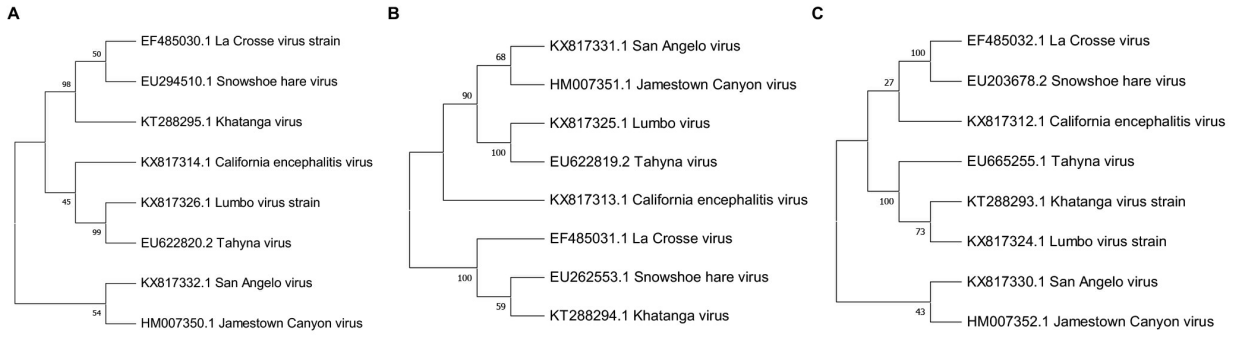

574

575 **Fig. 1 Phylogenetic trees of the S, M, L segments of LACV and related bunyaviruses.**

576 Phylogenetic trees were constructed from aligning nucleotide sequences of the A) small

577 (S), B) medium (M), and C) large (L) segments from bunyaviruses within the CSG, including

578 La Crosse virus, Snowshoe hare virus, Khatanga virus, California Encephalitis virus, San

579 Angelo virus, Lumbo virus, and Tahnya virus, and Melaka virus (MELV) family, including

580 Jamestown Canyon virus. The sequences were aligned using Clustal omega, and the

581 resulting alignments were used to construct maximum-likelihood trees based on the

582 Tamura-Nei model and 500 bootstrapping replications using Mega11. Associated

583 accession numbers are included by the name of each virus for each tree.

584

585

586

587

588

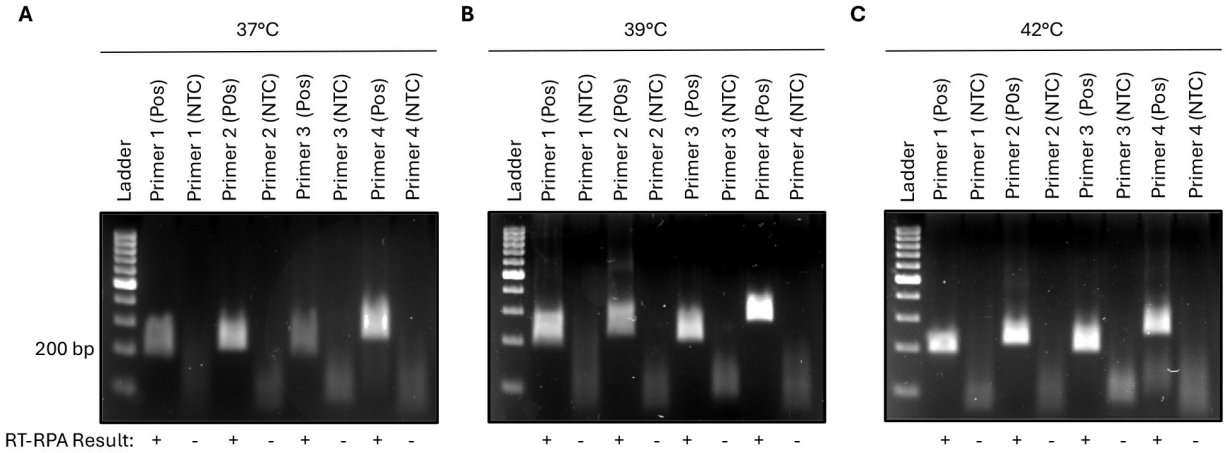

Fig. 2 Primer screen RT-RPA testing. Primer screen RT-RPA testing at A) 37°C, B) 39°C, and C) 42°C using 4 different primer pairs. Primer pair 3 at 39°C was chosen for further experimentation. The RT-RPA amplified products were not purified prior to running on the agarose gel. Pos, positive control, La crosse virus cDNA input. NTC, no template control, water input. +, positive result. -, negative result.

603

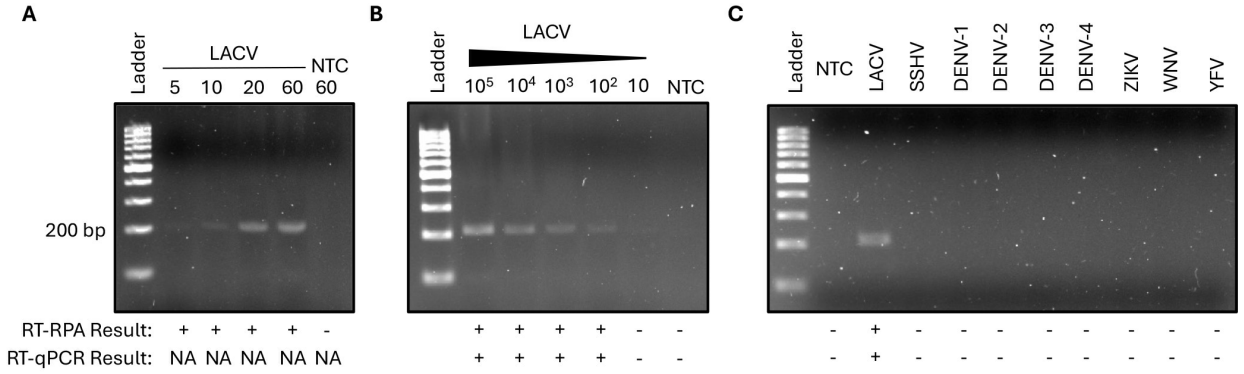

604

605 **Fig. 3 Time Course, limit of detection, and cross-reactivity RT-RPA testing with**

606 **visualization of results via gel electrophoresis.** A) Time course tests were performed at 5

607 minutes, 10 minutes, 20 minutes and 60 minutes. The time course was optimized at 20

608 minutes. RT-qPCR testing in the time course experiment was not applicable (NA). B) Viral

609 RNA from 10^5 copies to 0 copies was reverse transcribed to cDNA and used in RT-RPA and

610 RT-qPCR testing. The RT-RPA limit of detection was determined to be 100 viral copies. C)

611 RT-RPA was performed using cDNA from La Crosse virus (LACV), Snowshoe hare virus

612 (SSHV), dengue virus serotype 1 (DENV-1), dengue virus serotypes 2 (DENV-2), dengue virus

613 serotype 3 (DENV-3), dengue virus serotype 4 (DENV-4), Zika virus (ZIKV), West Nile virus

614 (WNV), or yellow fever virus (YFV). No cross-reactivity was observed. The RT-RPA products

615 were purified prior to running on the agarose gel. NTC, no template control, water input. +,

616 positive result. -, negative result.

617

618

619

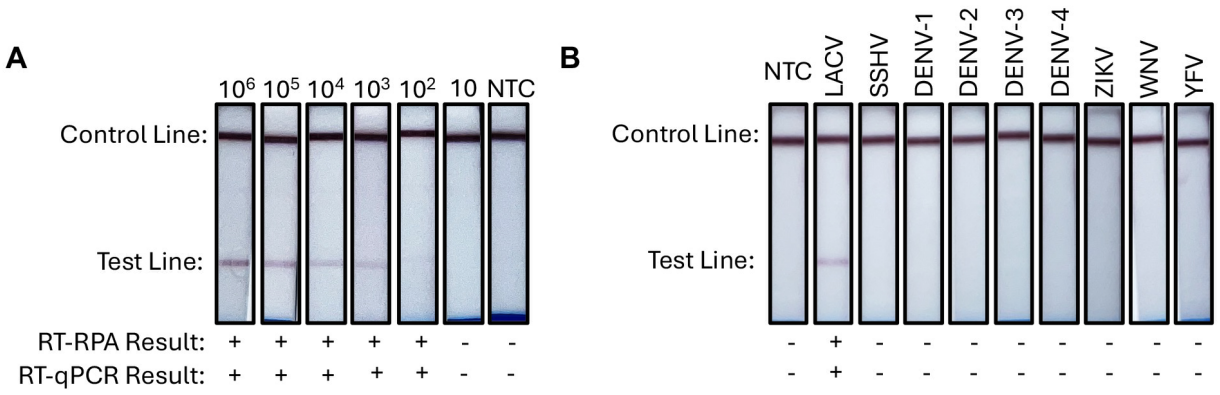

620

621 **Fig. 4. RT-RPA limit of detection and cross-reactivity testing with visualization of**

622 **results via LFA strips.** A) Viral RNA from 10^6 copies to 0 copies were reverse transcribed to

623 cDNA and used in RT-RPA and RT-qPCR testing. The limit of detection was determined to be

624 100 viral copies. B) RT-RPA and RT-qPCR testing was performed using cDNA from La Crosse

625 virus (LACV), Snowshoe hare virus (SSHV), dengue virus serotype 1 (DENV-1), dengue virus

626 serotypes 2 (DENV-2), dengue virus serotype 3 (DENV-3), dengue virus serotype 4 (DENV-4),

627 Zika virus (ZIKV), West Nile virus (WNV), or yellow fever virus (YFV). No cross-reactivity was

628 observed with either RT-RPA or RT-qPCR testing. NTC, no template control, water input. +,

629 positive result. -, negative result.

630

631

632

633

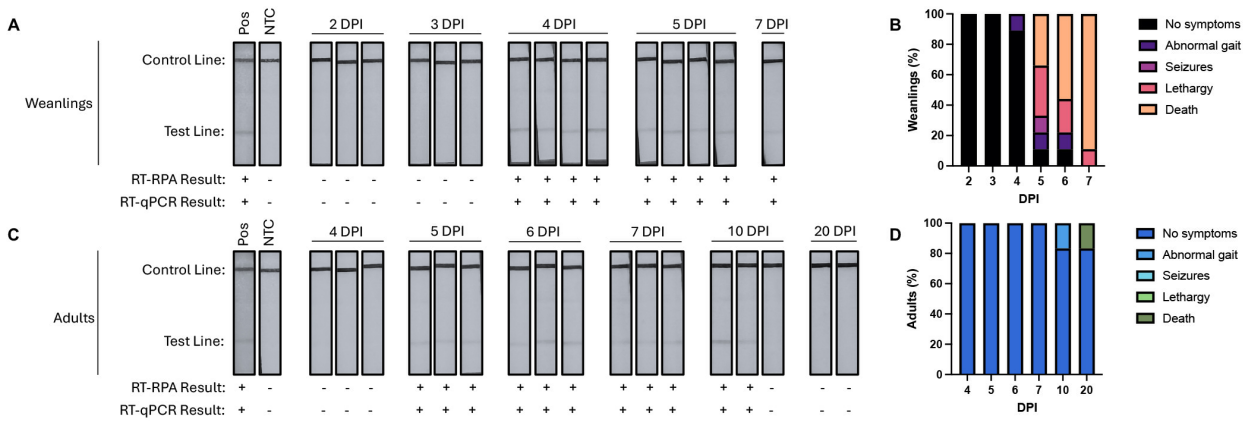

Fig. 5. LACV neuroinvasion into the brain of weanling and adult mice visualized by LFA strips. Mice were infected with 1000 plaque forming units of LACV and were humanely sacrificed and brains were collected 2-7 days post-infection (DPI) for weanlings and 4-20 DPI for adults. A) LACV was detected in the brain in weanling mice by both RT-RPA and RT-qPCR as early as 4 DPI. B) Bar chart representing percent weanling mice found with neurological symptoms. There was an onset of clinical symptoms by 4 DPI in weanlings, with worsening of neurological symptoms between 5-7 DPI. C) LACV was detected in the brain in adult mice by both RT-RPA and RT-qPCR by 5 DPI with clearance of the virus by 20 DPI. D) Bar chart representing percent adult mice found with neurological symptoms. There were no symptoms exhibited in adults between 4-7 DPI; however, one adult exhibited neurological symptom by 12 DPI and could not be included in the analysis. Two remaining adults were asymptomatic throughout the course of the study. Pos, positive control, La crosse virus cDNA input. NTC, no template control, water input. +, positive result. -, negative result.

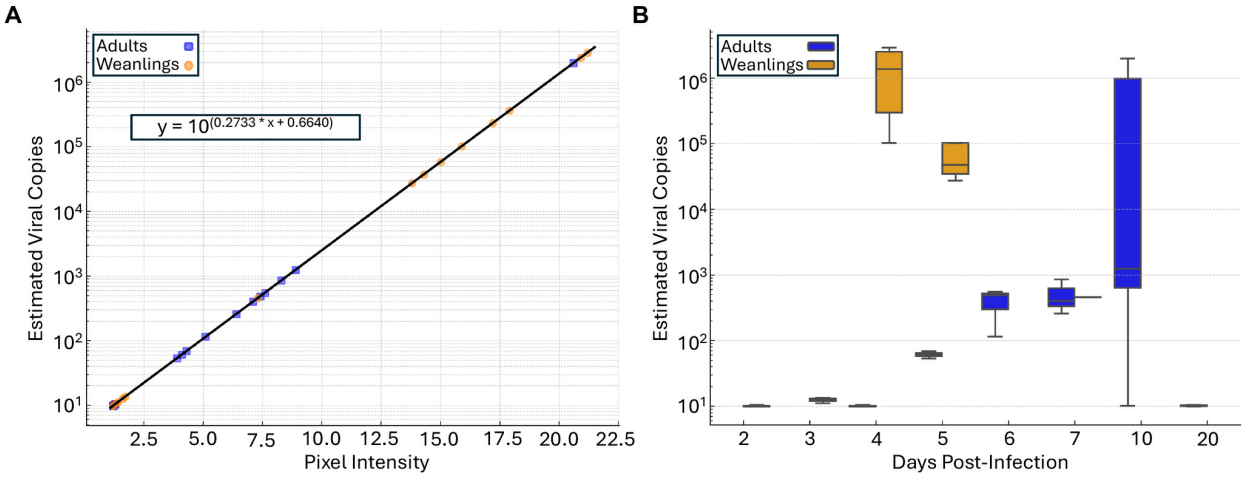

Fig. 6. Estimation of LACV viral burden in the brain from LFA strips. A) Test line pixel intensities for LACV-infected weanling (orange circles) and adult (blue squares) mice were plotted on the standard curve to estimate viral load dynamics over time. The standard curve is plotted as a black straight line, generated using linear regression (equation of the standard curve is included in the box). A logarithmic scale was used for viral copies to better represent dynamic changes in viral loads across multiple orders of magnitude. B) Box-and-whisker plot represents the distribution of estimated viral copies in weanlings (orange) and adults (blue) at each time point.

665 **Supplementary Figure**

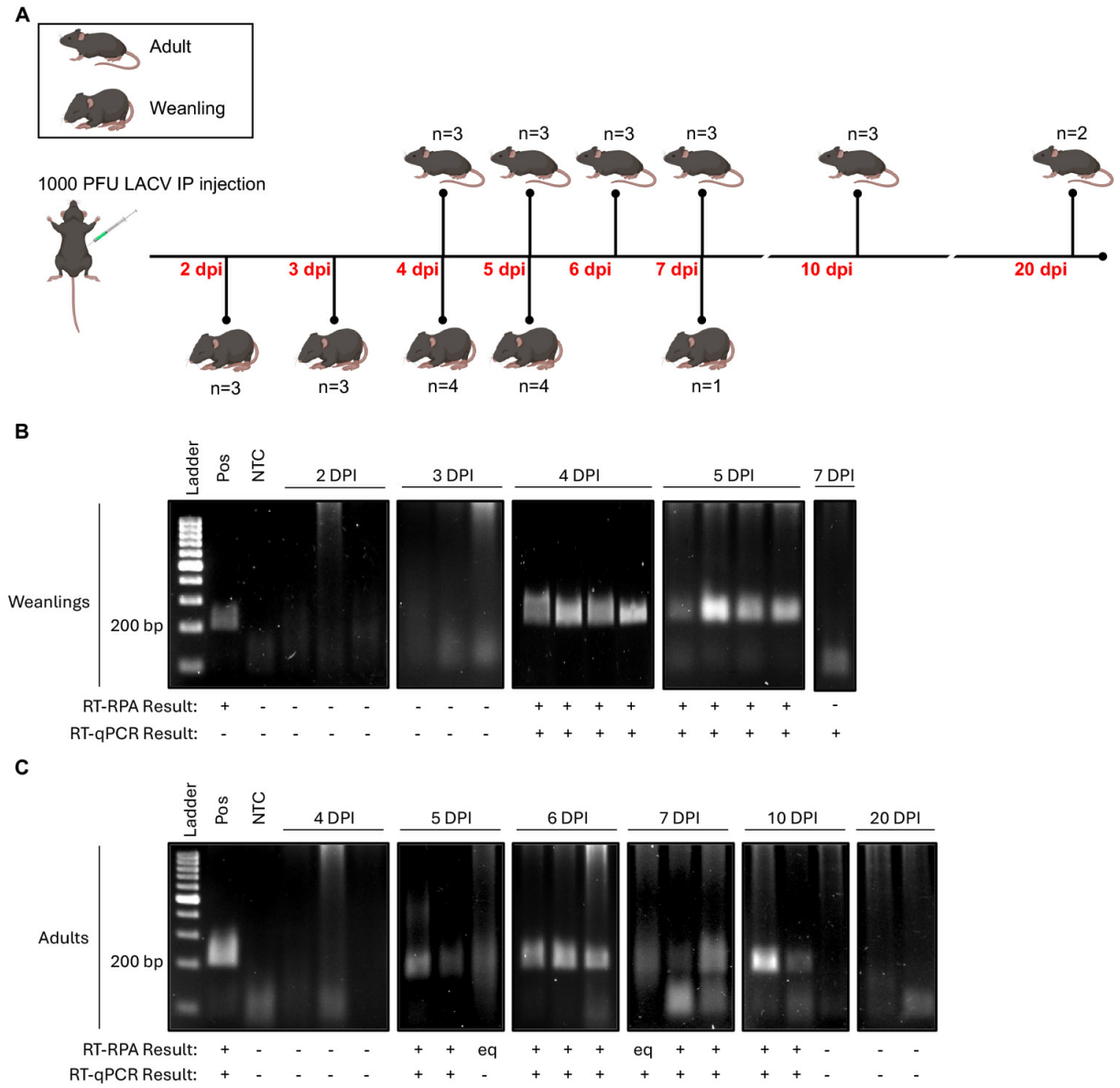

666

667 **Supplementary Fig. 1. Serial euthanasia schematic and LACV neuroinvasion into the**

668 **brain of weanling and adult mice visualized by gel electrophoresis.** A) Mice were

669 infected with 1000 plaque forming units of LACV and mice were humanely sacrificed, and

670 brains were collected 2-7 days post-infection (dpi) for weanlings and 4-20 dpi for adults. B)

671 LACV was detected in the brain in weanling mice by both RT-RPA and RT-qPCR as early as 4

672 DPI. The RT-RPA amplified products were not purified prior to running on the agarose gel. C)
673 LACV was detected in the brain in adult mice by both RT-RPA and RT-qPCR by 5 DPI with
674 clearance of the virus by 20 DPI. The RT-RPA amplified products were not purified prior to
675 running on the agarose gel. Pos, positive control, La crosse virus cDNA input. NTC, no
676 template control, water input. +, positive result. -, negative result. eq, equivocal result.

677

678

679

680

681

682

683

684

685

686

687

688

689

690 **Supplementary Table**

691 **Supplementary Table 1. RT-RPA primer pairs and hybridization probe.**

Primer Pair	Forward	Reverse	Amplicon Size
1	GTCTTGTTATCATTGGATTGTTGATCGGGCTGC	CCTGTGAGCCATCAAACCTGCAGCATCTTC	204
2	CAACCCAGCAAAGGCCTCAAACCTTGCTAGAGG	TGATCAGTGCTAGATTGGAATACACCACCTGATGG	228
3 (unlabeled)	**TGATTACCAAGCATGCAAATTCCTTCAAAGCCC**	**TTCGAAGCAGTTAATACAGCCGGTGCATGACCC**	**208**
3 (labeled reverse)	**TGATTACCAAGCATGCAAATTCCTTCAAAGCCC**	**/5Biosg/TTCGAAGCAGTTAATACAGCCGGTGCATGACCC**	**208**
4	CCTGACGTAAAGCTCATCCAAGAAGGCGATGGG	CGCTATGCTAGATCTGCTTACTTGCCAATTACAG	240
Hybridization Probe	**/56-FAM/GTGGCACTGTGACCATAA**		

692